Physical Review & Research International
3(3): 218-227, 2013

SCIENCEDOMAIN *international*
www.sciencedomain.org

Diagnostic of Laser Induced Li II Plasma

Banaz Omar[1*] August Wierling[1], Heidi Reinholz[1], and Gerd Röpke[1]

[1] *Institut für Physik, Universität Rostock, Universitätsplatz 3, 18051 Rostock, Germany*

Research Article

Received: 30 December 2012
Accepted: 26 February 2013
Published: 03 April 2013

Abstract

Spectral line broadening in dense plasmas is investigated for lithium He-like ion based on a microscopic quantum-statistical approach. By using thermodynamic Greens function, perturber-radiator interaction, plasma correlation and screening effects are taken into account. Ions are treated in quasi-static approximation, leading to a Stark effect by the surrounding perturbers microfield. Stark broadening of Li II $(2\mathrm{p}^3\mathrm{P}_{2,1,0}-2\mathrm{s}^3\mathrm{S}_1)$ 548 nm line is calculated, plasma parameters such as temperature and free electron density for the expanding Li plasma after 60 ns from laser irradiation are analyzed (Doria, D., Kavanagh, K.D., Costello, J.T., and Luna, H. (2006) Meas. Sci. Technol., 17, 670-674). The estimated spatial electron density and temperature ranges are $n_\mathrm{e} = (0.25-2)\times10^{24}\,\mathrm{m}^{-3}$ and T $\approx (2-3.5)$ eV, respectively. The dependence of plasma parameters on the line width is investigated. A good agreement is shown by comparing our calculation with the published measured profiles.

Keywords: Stark broadening; Greens function; plasma diagnostic

1 Introduction

Spectral line calculation is an interesting tool for plasma diagnostic. A radiating atom in dense plasmas is perturbed by the influence of surrounding particles, the perturbation leads to the shift and broadening of the line profile, the most dominating effect is Stark broadening. The diagnostic of the spatial and temporal distribution of plasma parameters in a laser-produced plasma is of great interest to many fields in science. Spectral line broadening of Li has industrial applications, lithium is used as a sources for EUV lithography and for soft x-ray emission. The plasma parameters, such as free electron density and temperature can be determined directly from calculated line profile in dense plasmas [1]. The temperature and density distributions are useful for fabrication of thin film materials such as high-temperature superconductors [2].

In this paper we analyze the experimental result of laser-produced Li II plasma at time delay 60 nm, the experiment have been carried out by Doria et al. [3]. Time and spatially resolved spectra

*Corresponding author: E-mail:banaz.omar@uni-rostock.de

is measured in one dimension along the plasma expansion normal to a Li target by using a time gated intensified charge-coupled device (ICCD) coupled to a stigmatic spectrometer. A Q-switched Nd:YAG laser at $\lambda = 1064$ nm is used with pulse duration 15 ns and 10 Hz repetition rate, the laser is focused onto a pure Li sample surface placed inside a vacuum chamber (5×10^{-5} mbar) generating a plasma that expands normal to the target surface. The laser irradiance is kept constant at an average of 1.3×10^{10} W cm^2. Laser-induced plasma parameters such as electron temperature, density and plume velocity are extracted directly from the image analysis which has been automated using a MATLAB code. The technique permitted rapid and ready characterization of laser plasma plumes in the early stage of the plasma expansion [3]. The temperature is determined from line intensity ratio of successively charged ions, which is the widely used technique. The spatial profile of the electron density is also estimated by using semiclassical perturbation formalisms from standard theory (ST) of Griem [1]. The ST is a semiclassical approach, where electrons are treated by using impact approximation with a cut-off procedure, while the interaction of ions at radiating particle is given in a quasi-static approximation due to the static microfield distribution function.

The quantum-mechanical Greens function method is considered in this paper to calculate the Li II spectral lines in dense plasmas, assuming local thermal equilibrium (LTE) [4-7]. In Sec. 2 an overview of the spectral line modeling is given. Result and discussion are shown in Sec. 3. Comparison with the experimental results of Doria et al. [3] is presented. Finally, conclusion is given in Sec. 4.

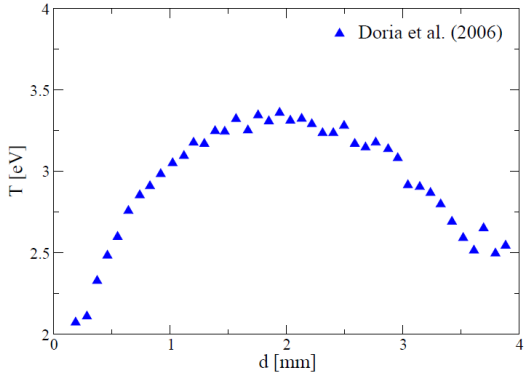

Figure 1: Estimated spatial temperature profile of Li II after 60 ns time delay in one dimension, d is the normal distance from the target surface, see Ref. Doria et al. [3].

2 Theoretical approach of pressure broadening in dense plasmas

Spectral line shape is given by the second order two-particle polarization function, which is a bound-bound transition. The polarization function is calculated in a systematic way from thermodynamic Greens function, which is proportional to the Fourier transform of the dipole-dipole autocorrelation function. The perturber-radiator interaction leads to a pressure broadening, which contains an electronic and an ionic contributions. Including the ionic contribution in the quasi-static approximation by averaging

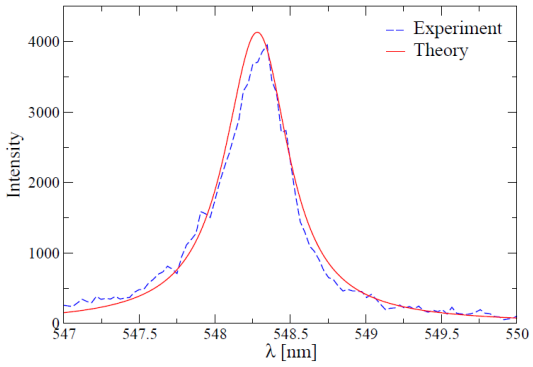

Figure 2: Pressure broadening of the line 548 nm Li II versus wavelength, theoretical profile at $n_e = 1.6 \times 10^{18}\mathrm{cm}^{-3}$ compared with the measurement [3] at $n_e = 1.885 \times 10^{18}\mathrm{cm}^{-3}$, $T = 2.46$ eV, and $d = 0.43$ mm.

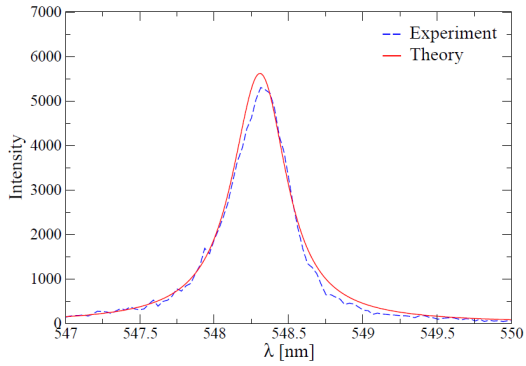

Figure 3: The calculated line profile of Li II 548 nm versus wavelength at $n_e = 1.376 \times 10^{18}\,\mathrm{cm}^{-3}$ and $T = 2.58$ eV. Comparison is made with the measured line [3] at estimated electron density $n_e = 1.38 \times 10^{18}\,\mathrm{cm}^{-3}$ and distance $d = 0.53$ mm.

over the ionic microfield [6], we have

$$I^{\mathrm{pr}}(\omega) \sim \sum_{i',i'',f',f''} \langle i'|\mathbf{r}|f'\rangle\langle f''|\mathbf{r}|i''\rangle \, \frac{\omega^4}{8\pi^3 c^3} \, \mathrm{e}^{-\frac{\hbar\omega}{k_{\mathrm{B}}T}} \int_0^\infty W(\beta)\, d\beta$$
$$\times \,\mathrm{Im}\, \langle i'|\langle f'|\left[\hbar\omega - \hbar\omega_{if} - \Sigma_{if}(\omega,\beta) + \mathrm{i}\Gamma^{\mathrm{v}}_{if}\right]^{-1} |f''\rangle|i''\rangle \quad , \tag{2.1}$$

where $\langle i|\mathbf{r}|f\rangle$ is identified as a dipole matrix-element for the transition between initial $n_i l_i m_i$ and final $n_f l_f m_f$ states. The vertex correction Γ^{v}_{if} for the overlapping line is related to coupling between the initial and the final states [4]. The ionic microfield distribution function $W(\beta)$ is taken according to Ref. [8] with field strength $\beta = E/E_0$ normalized to the Holtsmark field E_0, and $\hbar\omega_{if} = E_i - E_f$ is the unperturbed transition energy. The function $\Sigma_{if}(\omega,\beta)$ is determined by the self-energy correction $\Sigma_n(\omega,\beta)$ of the initial and the final states

$$\Sigma_{if}(\omega,\beta) = \mathsf{Re}\big[\Sigma_i(\omega,\beta) - \Sigma_f(\omega,\beta)\big] + \mathrm{i}\,\mathsf{Im}\big[\Sigma_i(\omega,\beta) + \Sigma_f(\omega,\beta)\big] \ , \tag{2.2}$$

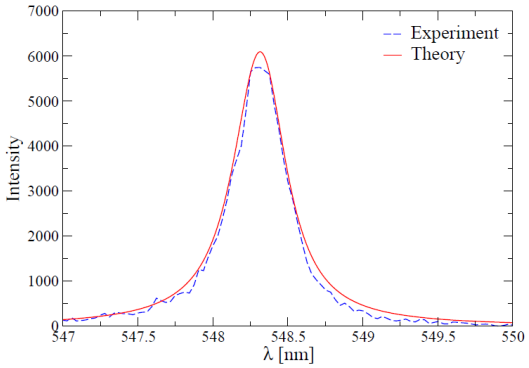

Figure 4: The calculated line shape of Li II 548 nm vs. λ at $n_e = 1.35 \times 10^{18}\,\mathrm{cm}^{-3}$ and $T = 2.69$ eV. Comparison is made with the measured profile in Ref. [3] at $n_e = 1.402 \times 10^{18}\,\mathrm{cm}^{-3}$ for the same temperature at distance $d = 0.6$ mm.

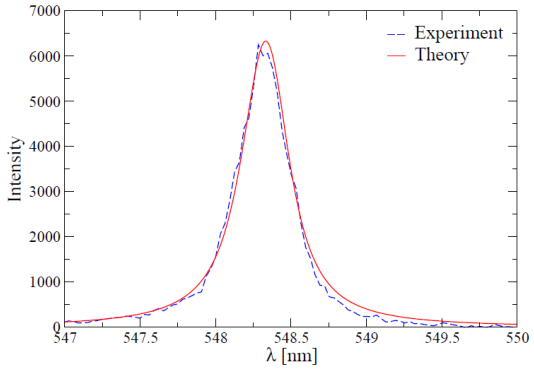

Figure 5: Stark broadening of the Li II line 548 nm versus wavelength. The calculated profile at $n_e = 1.2 \times 10^{18}\mathrm{cm}^{-3}$ compared with the measured one at $n_e = 0.982 \times 10^{18}\mathrm{cm}^{-3}$, $T = 2.77$ eV and $d = 0.676$ mm [3].

where the real part represents the shift Δ_n^{SE} and the imaginary part gives the width Γ_n^{SE} of each state. The electronic and ionic contributions occur in the self-energy

$$\Sigma_n(\omega,\beta) \;=\; \Sigma_n^{\mathrm{ion}}(\beta) + \Sigma_n^{\mathrm{el}}(\omega,\beta)\;. \tag{2.3}$$

Performing Born approximation with respect to the dynamically screened perturber-radiator potential, the electronic self-energy is obtained as

$$\begin{aligned}\Delta_n^{\mathrm{SE}} + \mathrm{i}\Gamma_n^{\mathrm{SE}} \;\;=\;\; < n|\Sigma^{\mathrm{el}}(E_n,\beta)|n >= -\frac{1}{e^2}\int \frac{\mathrm{d}^3q}{(2\pi)^3}V(q)\sum_\alpha |M_{n\alpha}(\mathbf{q})|^2 \\ \times \int_{-\infty}^{\infty}\frac{\mathrm{d}\omega}{\pi}[1+n_{\mathrm{B}}(\omega)]\frac{\mathrm{Im}\,\varepsilon^{-1}(\mathbf{q},\omega+\mathrm{i}0)}{E_n - E_\alpha(\beta) - \hbar(\omega+\mathrm{i}0)}\;.\end{aligned} \tag{2.4}$$

Here, the level splitting ($E_\alpha(\beta) \approx E_\alpha$) due to the microfield has been neglected [5], $n_{\mathrm{B}}(\omega) = \left[\exp(\hbar\omega/k_{\mathrm{B}}T) - 1\right]^{-1}$ is the Bose distribution function, and the sum over principal quantum number

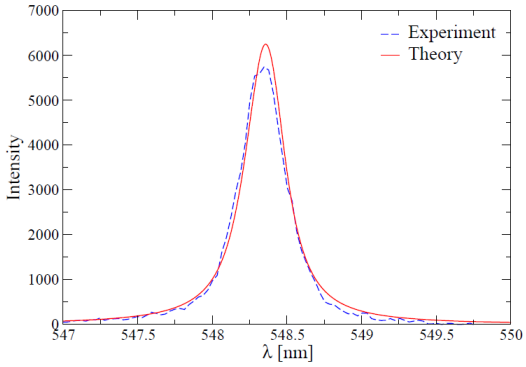

Figure 6: Comparison of the theoretical and measured line shapes of the Li II 548 nm line vs. wavelength at $n_e = 1.0 \times 10^{18}\mathrm{cm}^{-3}$ and $n_e = 0.962 \times 10^{18}\mathrm{cm}^{-3}$, respectively, at $T = 2.96$ eV and $d = 0.89$ mm [3].

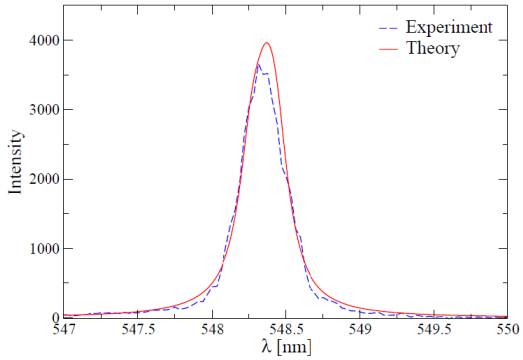

Figure 7: The line profiles of Li II 548 nm line versus wavelength. Our calculation at $n_e = 0.8 \times 10^{18}\mathrm{cm}^{-3}$ compared with the profile measured in Ref. [3] at $n_e = 0.561 \times 10^{18}\mathrm{cm}^{-3}$, $T = 3.3$ eV, and $d = 1.53$ mm.

α runs from $n-2$ to $n+2$ discrete bound states for the virtual transitions. Dynamical screening effect is accounted for in Eq. (2.4) from imaginary part of the inverse dielectric function $\varepsilon^{-1}(\mathbf{q},\omega)$, which is approximated by random phase approximation (RPA). The transition matrix-element $M_{n\alpha}(\mathbf{q})$ describes the interaction of the atom with the Coulomb potential through the vertex function, where the Coulomb interaction with electron-electron-ion triplet depends on the momentum transfer $\hbar\mathbf{q}$ [4]. The matrix-element of He and He-like ions can be approximated by the one of hydrogen, while the outer electron is screened by inner electron [7]. The electronic wavefunction for singly ionized Li is obtained by applying Coulomb approximation method [9]. In this approximation the wavefunction and radial part of the transition matrix-element are expressed in terms of $[P_{nl}(r) = r\,\psi_{nl}(r)]$ and σ, respectively. To verify the wavefunction, the absorption oscillator strength of transition f_{if} and σ^2 of the singly excited states of Li II are indicated as [10-13]

$$f_{if} = \frac{1}{3}\frac{\Delta E}{R}\frac{\max(l_i, l_f)}{2l+1}\left(\int_0^\infty r\,P_{n_i l_i}(r)\,P_{n_f l_f}(r)\,dr\right)^2, \tag{2.5}$$

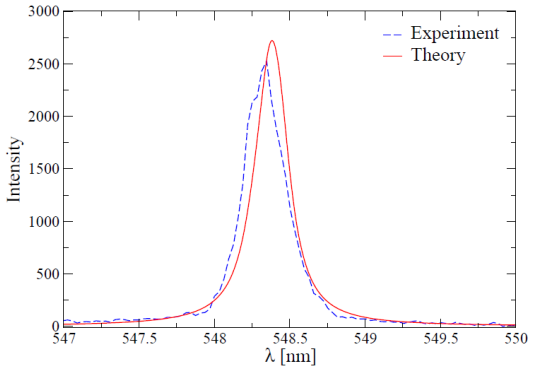

Figure 8: The line profiles of Li II 548 nm line vs. wavelength. Our calculation at $n_e = 0.76 \times 10^{18}\mathrm{cm}^{-3}$ compared with the profile measured in Ref. [3] at $n_e = 0.43 \times 10^{18}\mathrm{cm}^{-3}$, $T = 3.31$ eV, and $d = 2.02$ mm.

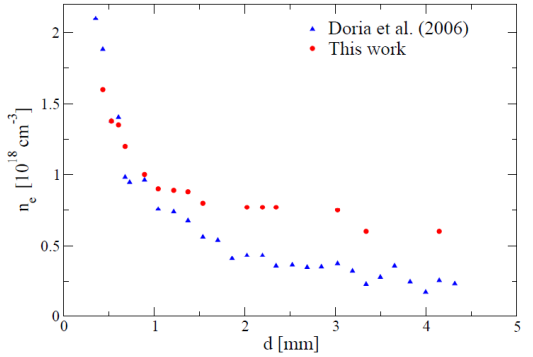

Figure 9: The free electron density distribution of Li II versus normal distance from the sample surface d. Comparison is made with the estimation values in Ref. [3] at 60 ns delay time.

where R is the reduced mass Rydberg constant, and ΔE is the transition energy.

Considering Born approximation, the electronic part is overestimated, to avoid this we apply the cut-off procedure and add a strong collision term [1,14,15] in stated of partial summation of the three-particle T-matrix, where the result might be slightly modified. For Li II we adopt the cut-off parameter $\rho_{\min} = n^2/Z$, where Z is the effective charge [14]. The close electron-radiator collision term ϕ_{SC} is evaluated according to the semiclassical estimation in Refs. [14-17]

$$\phi_{\mathrm{SC}} = -\frac{4\pi}{3}\left(\frac{2m_e}{\pi k_{\mathrm{B}} T}\right)^{1/2} n_e \left(\frac{\hbar}{m_e}\right)^2 | < nl|r|nl > |^2 C_{nl}\,, \tag{2.6}$$

where C_{nl} is the strong collision constant and $< nl|r|nl >$ is the dipole matrix-element.

For non-hydrogenic radiator, ionic contribution to the self-energy is related to quadratic Stark effect and quadrupole interaction, further detail is given in Refs. [6,7]. The microfield can be considered as a static microfield distribution function, while it does not change during the time of interest for the radiation process.

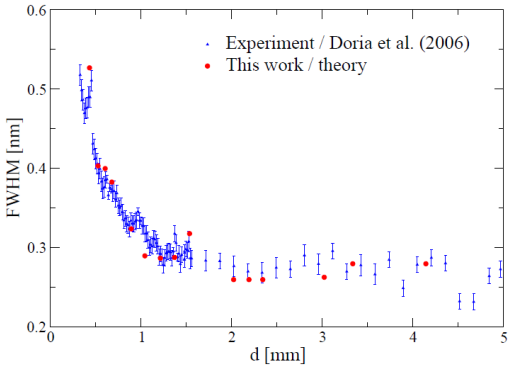

Figure 10: The FWHM of Li II ($2\mathrm{p}^3\mathrm{P}_{2,1,0} - 2\mathrm{s}^3\mathrm{S}_1$) 548 nm line versus distance. Comparison is made with the estimated values from measured profiles after 60 ns laser exposure [3].

3 Results and Discussion

In this section, we perform the pressure line broadening and the related full width at half maximum (FWHM) of the Li II 548 nm line by applying the approach outlined above. The comparison between our theoretical calculation and experimental results is shown, assuming LTE. The time-resolved measured profiles are space resolved along the direction of expansion, the observed plasma parameters such as relative line intensities and Stark broadening parameters have been extracted from the profiles [3]. Under the assumption of LTE, the spatial electron temperature profile is evaluated from the intensity ratio of Li II at two isolated lines 548 nm and 467 nm, see Fig. 1 **??**3,18]. The relative intensities are corrected according to the wavelength dependence of the spectral sensitivity of the spectrometer. The statistical error in the intensity ratio is less than 3% for distances between $d = 1$ mm to $d = 3$ mm from the sample surface, but increased up to 10% further away at the edges of the plasma plume, where distance $d = 0$ at the target surface. Considering an initial plasma temperature of 8.6 eV gives the velocity of 1.99×10^5 cm/s at 60 ns time delay. The spatial distribution of the density ratio between Li ions and atoms is obtained in Ref. [3] by using the Saha equation. Two different regions can be defined, $d < 2$ mm and $d > 2$ mm where the electron temperature reaches its maximum value, see Fig. 1. The first region is a sharp transient in the $n_{\mathrm{ion}}/n_{\mathrm{atom}}$ density ratio, mostly driven by the rapid change in the electron density, this can be clearly seen in Fig. 9. However, in the second region the density ratio becomes constant, indicating that the plasma has reached thermal equilibrium between the ion and atom populations, while in this stage the electron density is almost constant and the temperature begins to drop, for more detail see Ref. [3].

Stark broadening parameters are calculated from Eq. 2.4 by using thermodynamic Greens function, the cut-off procedure is adopted and the strong collision term is added by using Eq. 2.6 according to Griem and his collaborators [14,15]. The ionic contribution is taken into account from second-order perturbation theory which is known as the quadratic Stark effect [11]. Ions are treated in quasi-static approximation by using microfield distribution function of Hooper [8], the comparison is done with the distribution function given in Ref. [19], where no sensible difference has been observed. The pressure line broadening is evaluated from Eq. 2.1 and compared with the measurement [3], given in Figs. 2-8. Then the electron density and the FWHM are estimated from the best-fitting profile with the measurement, illustrated in Figs. 9 and 10, respectively. The plasma expands freely and cooling down while the electron density decreases with increasing d normal to the surface. The gradient of density as a function of d in one dimension after 60 ns of laser exposure is shown in Fig. 9. The electron density profile is indicated in Ref. [3] from line broadening by extrapolating the tabled

values of Griem [1]. The highest value of the electron density observed near the target surface, by plasma cooling n_e decreases rapidly with increasing d due to condensation and recombination. In Fig. 9 the variation of n_e near the surface is in a good agreement with the estimation in Ref. [3], while the discrepancy can be seen with increasing d, this can be clearly seen in Fig. 8. The Doppler broadening becomes less important with increasing density, and the width is only due to Stark broadening at high density. Regarding the data reported in Ref. [3], the discrepancy may be due to the self-absorption.

The accuracy of calculating electronic dipole matrix-elements is approved by comparing our results of the radial part of transition matrix-element σ^2 and the oscillator strength of transition f_{if} with the other calculated values in Ref. [12,13,20], see table 1, very good agreement can be seen.

Transition		σ^2	$\sigma^{2\,(1)}$	f_{if}	$f_{if}{}^{(1)}$	$f_{if}{}^{(2)}$
^{3}S-^{3}P^0	2s-2p	1.85014	1.894	0.307485	0.323	0.30665/0.307940
	-3p	0.240332	0.2361	0.182895	0.179	0.18330/0.1871
	-4p	0.0627511	0.0578	0.0605617	-	0.05637/0.0575
	3s-2p	0.210062	0.2201	0.115857	-	0.11416/0.11710
	-3p	11.8357	11.93	0.512237	-	0.51167/0.5128
	-4p	0.7274	0.7274	0.179942	-	0.18583/0.18686
	4s-2p	0.0270884	0.0280	0.0211708	-	0.020787/0.02147
	-3p	1.36309	1.413	0.254529	-	0.25376/0.2550
	-4p	40.69	40.69	0.706735	-	0.70298/0.7036

Table 1: Comparison is given between our calculated values of the radial part of transition matrix-element σ^2 and the oscillator strength of transition f_{if} for triplet transition of Li II and those in Refs. $^{(1)}$[12] and $^{(2)}$[13].

4 Conclusions

In this study, diagnostic of laser induced lithium plasma by Doria et al. [3] is performed. The quantum statistical approach is presented to the line profile calculation of allowed isolated Li II 548 nm, this method is applicable for both allowed and forbidden radiative transitions. A cut off procedure is used for strong collisions according to Griem [1]. The Coulomb approximation is employed to evaluate the wavefunctions of Li II. In our calculation, the time-dependent microfield fluctuation is approximated by its static value due to the large mass of the ion relative to the electron mass, assuming the stationary motion of ions during the time of collisions. The contribution of ions is taken into account within quadratic Stark effect in the quasi-static approximation. The spatial distribution of the electron density is estimated along the direction of plasma plume expansion. Good agreement can be clearly seen by comparing our line profiles with the measured profiles. However, the estimated values of n_e in Ref. [3] are overestimated systematically with increasing distance.

Acknowledgment

This work is supported by SFB 652.

Competing interests

The authors declare that no competing interests exist.

References

1. Griem HR. Spectral Line Broadening by Plasmas. New York: Academic Press; 1974.

2. Bäuerle D. Pulsed-laser deposition and characterization of high-temperature superconductors. Supercond. Sci. Technol. 1998;11:968-972.

3. Doria D, Kavanagh KD, Costello JT, Luna H. Plasma parametrization by analysis of time-resolved laser plasma image spectra. Meas. Sci. Technol. 2006;17: 670-674.

4. Kraeft WD, Kremp D, Ebeling W, Röpke G. Quantum Statistics of Charged Particle Systems. Berlin: Akademie-Verlag; 1986.

5. Günter S, Könies A. Quantum mechanical electronic width and shift of spectral lines over the full line profile-electronic asymmetry. Quant. Spectrosc. Radiat. Transfer. 1994;52:819-824.

6. Sorge S, Wierling A, Röpke G, Theobald W, Sauerbrey R, Wilhein T. Diagnostics of a laser-induced dense plasma by hydrogen-like carbon spectra. J. Phys. B: At. Mol. Opt. Phys. 2000;33:2983-3000.

7. Omar B, Günter S, Wierling A, Röpke G. Neutral helium spectral lines in dense plasmas. Phys. Rev. E. 2006;73:056405-13.

8. Hooper CF Jr. Low-frequency component electric microfield distribution in plasmas. Phys. Rev. 1968;165:215-222.

9. Bates DR, Damgaard A. The calculation of the absolute strengths of spectral lines. Phil. Trans. Roy. Soc. London A. 1949;242:101-122.

10. Wiese WL, Fuhr JR. Accurate Atomic Transition Probabilities for Hydrogen, Helium, and Lithium. Published online 24 June 2009; publisher error corrected 23 September 2009.

11. Bethe HA, Salpeter EE. Quantum Mechanics of One- and Two- Electron Atoms. New York: Plenum Publishing Corporation; 1977.

12. Cohen M, Kelly PS. Hartree-Fock wave function for excited states. IV. oscillator strength in the helium isoelectronic sequence. Can. J. Phys. 1967;45:2079.

13. Theodosiou CE. Lifetimes of the Singly Excited States in Li I I. Physica Scripta. 1985;32:129-133.

14. Griem HR. Shifts of hydrogen and ionized-helium lines from $\Delta n = 0$ interactions with electrons in dense plasmas. Phys. Rev. A. 1988;38:2943-2952.

15. Griem HR, Blaha M, Kepple PC. Stark-profile calculations for resonance lines of heliumlike argon in dense plasmas. Phys. Rev. A. 1990;10:5600-5609.

16. Griem HR, Blaha M, Kepple PC. Stark-profile calculations for Lyman-series lines of one-electron ions in dense plasmas. Phys. Rev. A. 1979;19:2421-2432.

17. Nguyen H, Koenig M, Benredjem D, Caby M, Coulaud G. Atomic structure and polarization line shift in dense and hot plasmas. Phys. Rev. A. 1986;33:1279-1290.

18. Griem HR. Plasma Spectroscopy. New York: McGraw-Hill; 1964.

19. Sadykova S, Ebeling W, Valuev I, Sokolov I. Electric microfield distributions in Li^+ plasma with account of the ion structure. Contr. Plasma Phys. 2009;49:76-89.

20. Ateş Ş, Çelik G. Oscillator Strengths for Allowed Transitions in Li II. Acta Physica Polonica A. 2009;116:169-175.

Peer-review history:
The peer review history for this paper can be accessed here (Please copy paste the total link in your browser address bar)
www.sciencedomain.org/review-history.php?iid=216&id=4&aid=1203